JMATPRO	Journal of Advanced Materials and Processing 9 (3): 47-53, Summer 2021 http://jmatpro.iaun.ac.ir 20.1001.1.2322388.2021.9.2.6.4

Research Paper

Effects of Active Material Particles Size Distribution on the Fabrication of $TiNb_2O_7$ Electrode Used in Lithium-Ion Batteries

Touraj Adhami[1], Reza Ebrahimi-Kahrizsangi[1], Hamid Reza Bakhsheshi-Rad[1*], Somayeh Majidi[2], Milad Ghorbanzadeh[3]**

1. Advanced Materials Research Center, Materials Engineering Department, Najafabad Branch, Islamic Azad University, Najafabad, Iran

2. Department of Chemistry, Najafabad Branch, Islamic Azad University, Najafabad, Iran

3. Materials and Energy Research Center, Karaj, Iran

ARTICLE INFO

Article history:

Received 14 March 2021
Accepted 18 May 2021
Available online 1 July 2021

Keywords:
Anode materials
particle size
uniform distribution
Li ion battery
electrode

ABSTRACT

In this study effect of active material particle size distribution (PSD) on $TiNb_2O_7$ electrodes and their performance were evaluated. To determine the effect of PSD, have focused on the performance of the electrode, which is mainly affected by the performance of individual particles and their interaction. For this purpose, $TiNb_2O_7$ was successfully synthesized by mechanochemical method and post-annealing, as an anode material for lithium-ion batteries. Phase identifications and microstructure characterization was carried out by X-ray diffraction (XRD) and field emission scanning electron microscopy (FESEM) to identify the phases and evaluate the morphology of the synthesized samples. The charging and discharging tests were conducted using a battery-analyzing device for evaluating the electrochemical properties of the fabricated anodes. Eventually, at faster charging rates, the electrochemical performance was found to be improved when smaller active material particle size distribution was used. Differences in particles size distributions resulted in variable discharge capacities so that the sample with particle size higher than 25 microns (>25 μm) showed a capacity of 19 mAh/g after 179 cycles, which had a lower capacity than their sample with particle size less than 25 microns (<25 μm). The final capacity of the sample with a particle size less than 25 microns is 72 mAh/g.

Citation: Adhami, T.; Ebrahimi-Kahrizsangi, R.; Bakhsheshi-Rad, H.R.; Majidi, S.; Ghorbanzadeh, M. (2021) Effects of Active Material Particles Size Distribution on the Fabrication of TiNb2O7 Electrode Used in Lithium-Ion Batteries, Journal of Advanced Materials and Processing, 9 (3), 15-22. Dor: 20.1001.1.2322388.2021.9.2.6.4

*[*] **Corresponding Author:**
E-mail Address: : rezaebrahimi@iaun.ac.ir, rezabakhsheshi@gmail.com

1. Introduction

Nowadays, intermediate metal oxides with high specific capacity and good cyclability in the anode materials development used in lithium-ion batteries have been extensively studied [1,2]. Among these, $TiNb_2O_7$ chemical composition was considered by many researchers [3,4] due to their unique characteristics such as high theoretical capacities of 387 mAh/g (much more than $Li_4Ti_5O_{12}$: 175 mAh/g), the process of rapid insertion and extraction of lithium-ion owing to rapid reaction kinetics, and high operating voltage (~1.6 sv, Li/Li^+) which can prevent the formation of solid electrolyte interface (SEI) layer. However, the operating discharge of these materials is not quite satisfactory due to their weak electric conductivity and the slow rate of ion transfer [3-5]. Various approaches and strategies, including reducing the particles size and improving the specific area, and designing the porous structures, were investigated to address this issue since a higher specific area shortens the distance for penetration of lithium ions, improves the electric conductivity, and will consequently improve the lithium ions storage performance [4,6]. However, an important fact that is often overlooked in electrode fabrication is the electrode particle size and the narrow distribution of particle size at the electrode surface. The broad and dissimilar particle sizes, active material particles are not similar in terms of morphology and size, and therefore have a heterogeneous system at its highest level. The degradation of Li-ion batteries is related to the particle size distribution (PSD) of the active material. In graphite anodes, solvent co-intercalation can cause particles to crack, and gas evolution leads to the same thing as well [7,8]. Moreover, in case of any changes in the volume of particles, contact loss will happen between particles [9]. Various materials show the agglomeration of particles in Li-ion batteries [6-8], and this is particularly significant and critical for those materials with considerable variations in their volumes [10] or use nanosized particles [8]. Therefore, although it has been proven in the discussion of making lithium-ion batteries that reducing the particle size improves its performance, while the actual shape and size distribution effect is often not examined. The PSD of the active material is a well-known property in Li-ion batteries and can be adjusted during the manufacture of battery electrodes [11,12]. Therefore, in order to better and more accurately understand the subject, the particle size distribution of active materials at the electrode surface and its effect on the performance of $TiNb_2O_7$ anode will be investigated in this research.

2. Experimental Procedure

$TiNb_2O_7$ ceramic powder was produced as the following reaction:

$$TiO_2 + Nb_2O_5 \rightarrow TiNb_2O_7 \quad (1)$$

N_2O_5 (99. 5% purity, particles size 25 μm) and TiO_2 (99% purity, < 2 μm) were the raw materials used to reach this goal. The purchase of the whole chemical was from Merk, and none of them were purified. To perform the MA process, a high-energy planetary ball mill was used with hardened chromium steel vials (vol. 125 ml) and balls (15 and 20 mm in diameter) while the purity of the argon atmosphere under which the process was performed was high. The speed of rotation was set up to 600 rpm. The ball-to-powder weight ratio (BRP) was considered 15:1, where the total mass of the powder was 7 g. Every 45 minutes, the milling planetary is stopped for 15 minutes so that the temperature will not be rising. The milling time was equal to 5 hours. In the next step to complete the chemical reactions and remove the raw materials, Samples were annealed in a tube furnace under an oxygen atmosphere for 2 hours at 900 °C. Evaluating the phase and crystallographic structural properties of the nano-powder; the X-ray diffraction was used. The collection of the XRD patterns was performed over the 2θ angular range between 20 and 60 at a scan rate of 1°/min. XRD data was needed to be analyzed, the PANalytical X'Pert High Score software can be used. We can compare the XRD patterns and standards to those standards which are compiled by the Joint Committee on Powder Diffraction and Standards (JCPDS), #01-070-2009 for $TiNb_2O_7$, #01-072-0158 for $Ti_2Nb_{10}O_{29}$, #01-071-1168 for TiO_2, and #01-030-0873 for Nb_2O_5. The morphological features of $TiNb_2O_7$ nano-powders were examined on a Field emission scanning electron microscope (FESEM; Vega©-Tescan, Brno, Czech Republic) that operated at the acceleration voltage of 15 kV. Energy-dispersive X-ray spectrometry (EDS) attached to the FESEM was also utilized for semi-quantitative examination of the samples. To determine the volume fraction of grain boundary of the nano-powders, the edge-mode of the FESEM images was employed. After the production of $TiNb_2O_7$ nano-powder, the synthesized powder was divided into two parts to investigate the uniform particle size distribution effect of active materials on the electrochemical performance of the anode (Table 1). Then a group of samples passed through a screen with 500 mesh (< 25 μm) and then entered the electrode manufacturing stage. While the other group entered the slurry and electrode production stage directly without passing through the screen.

Table 1. Specifications of the applied parameters in the experimental process.

Sample No.	Stoichiometric reaction	Milling time (h)	Furnace/annealing atmosphere	Annealing time (h)	Annealing temperature (°C)	Screen
N1	$TiNb_2O_7$	5	Tube/oxygen	2	900	Yes
N2	$TiNb_2O_7$	5	Tube/oxygen	2	900	No

Lithium-ion storage performance in the compositions of $TiNb_2O_7$ was investigated using the $Li/TiNb_2O_7$ half-cells. When each of the synthesized materials is mixed with polyvinylidene fluoride (PVDF), and black carbon, which acts like the adhesive and conductor, weight ratio 70:15:15 inside N-Methyl-2-pyrrolidone (MNP), the electrodes that are used at practical work can be produced. The slurry we gained covered a copper foil, and this was then dried for 12 hours under the temperature of 120 °C inside an oven under vacuum condition. In each half-cell, the ande material was loaded at a rate of 1 mg/cm^2 in accordance with the previously performed work [13,14]. The separator used in this study was a thin layer (film) of polypropylene (Celgard 2400). A standard vacuum glovebox with a pure lithium foil as a cathode/ counter in the coin cells was used to mount each of the prepared anodes inside it (CR 2032). Combining one molar LiPF6 in ethylene carbonate (EC), diethyl carbonate (DEC), and dimethyl carbonate (DMC), the preparation of the used electrolytes took place. A battery analyzer (BTS4000 5V) device by galvanostatic cycles in the voltage range of 0 to 3 volts at room temperature was used to perform charging and discharging tests. Then, an electrochemical impedance test was used to calculate the diffusion coefficient of lithium-ion in each half cell. The equation used to calculate the diffusion coefficient is as follows [14]:

$$D = R^2T^2/2A^2n^4F^4C^2\sigma_w^2 \quad (2)$$

where R is the gas constant (8.314 J/mol K), T is the absolute temperature, n is the number of electrons exchanged in each molecule during the redox process, A is the surface area of the electrode (1.77 cm^2), C is the lithium-ion concentration (7.69×10^{-13} mol.cm^{-3}), F is the Faraday constant (96486 C/mol), and σ_w is a Warburg factor that is directly related to Z', as follows:

$$Z' = R_e + R_{ct} + \sigma_w^{-1/2} \quad (3)$$

where Z' is the real part of the electrochemical impedance test, indicating the general resistance of the cell, R_e represents the resistances due to the electrode and electrolyte, and R_{ct} is the charge transfer resistance.

3. Results and Discussion:

3.1. Phase analysis and structural features

Fig. 1 shows the X-ray diffraction pattern of the powder sample synthesized before and after the annealing process. According to Fig. 1a, the un-annealed sample was composed of TiO_2 and Nb_2O_5 [13]. Besides, several product peaks corresponding to $TiNb_2O_7$, $Ti_2Nb_{10}O_{29}$, and $TiNb_{24}O_{62}$ were detected. Compounds of $TiNb_2O_7$, $Ti_2Nb_{10}O_{29}$, and $TiNb_{24}O_{62}$ all belong to the same family, which are obtained by reacting between TiO_2 and Nb_2O_5 with different stoichiometry. Therefore, phase overlap is strongly observed between these three compounds. The XRD patterns of the annealed products are shown in Fig. 1b [13]. It can be seen that the characteristic peaks of TiO_2 and Nb_2O_5 were completely removed in the annealing process. Based on clearly defined X-ray patterns, annealing operations lead to the completion of the chemical reaction and the removal of raw materials peaks.

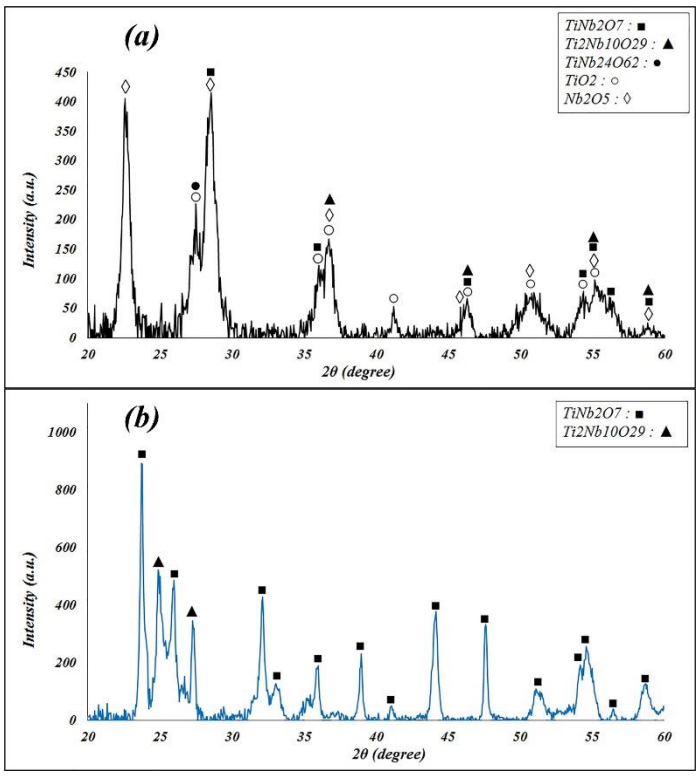

Fig. 1. Diffracted X-ray patterns of the compounds $TiNb_2O_7$: (a) before annealing (b) after annealing [13].

3.2. Morphological evaluations characteristics

Fig. 2 shows an image of the synthesized $TiNb_2O_7$ powder before the electrode was made. In this figure, the agglomeration of particles is observed. The agglomeration phenomenon has occurred due to the reduction of particle size caused by milling and the increase in the surface defects, which results in an unstable surface, and with a longer milling time, the system will reach a stable state. The surface diameter size of the synthesized particles is in the range of 13 to 24 nm. The EDS analysis and elemental mapping were used to understand the XRD results better, as shown in Fig. 3. According to the EDS spectrum (Fig. 3a), the main components of the nano-powder in terms of the element were oxygen, niobium, and titanium. From elemental mapping analysis (Fig. 3b), the nano-powder showed a homogenous distribution of O, Nb, and Ti elements which confirmed the formation of a uniform microstructure after annealing.

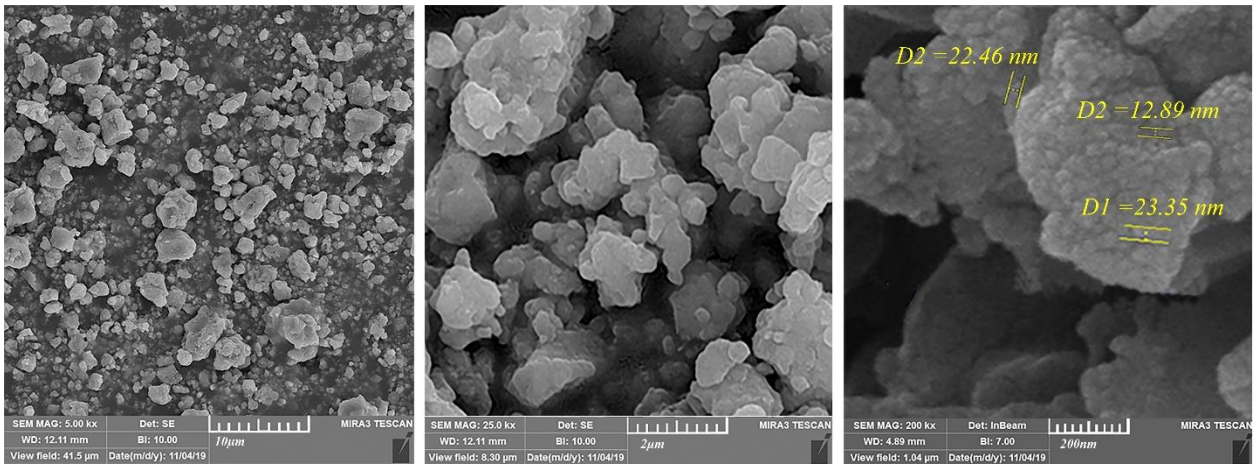

Fig. 2. The morphological features of the $TiNb_2O_7$ nano-powders.

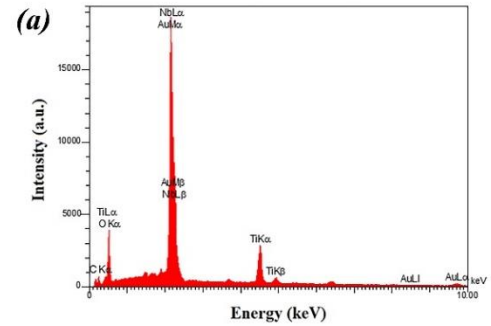

Elt	Line	Int	Error	W%	A%
C	Ka	40.1	126.4178	4.33	13.12
O	Ka	260.4	126.4178	27.26	62.06
Ti	La	34.5	126.4178	2.22	1.69
Nb	La	1772.1	125.7339	52.53	20.60
Au	Ma	443.0	125.7339	13.67	2.53
				100.00	100.00

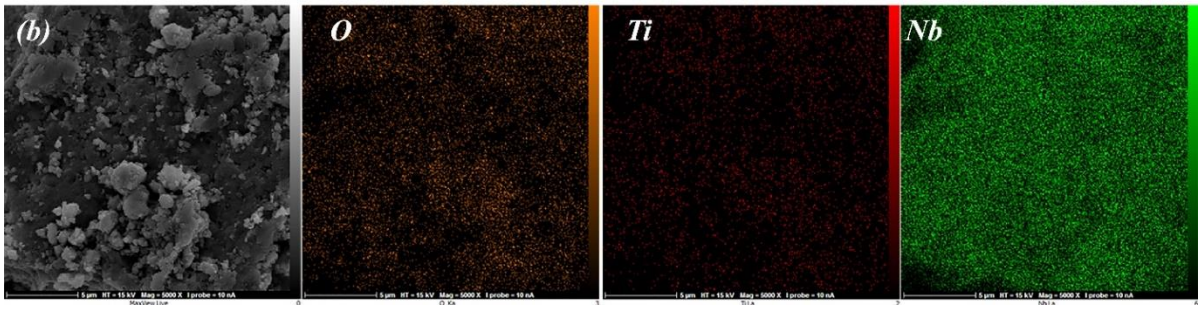

Fig. 3. (a) EDS analysis and (b) elemental mapping images of $TiNb_2O_7$ sample

3.3. Charging and discharging curves

To investigate the effect of particle size distribution on the electrochemical performance of $TiNb_2O_7$ anodes, the made electrodes were charged and discharged during 179 cycles at different C rates (Table 2). Fig. 4 shows a comparison graph of the discharge diagrams of the two samples N1 and N2. As can be seen at all C rates, the performance of the sample (with uniform particle size distribution) is much better than that of the sample containing non-uniform particle distribution, so that the difference in the final capacity at the end of each C rate, including 0.1C, 0.2C, 0.5C, 1C, 2C, and 4C is equal to 45, 50, 73, 73, 62 and 53 mAh/g, respectively. In other words, the yield of a heterogeneous sample (N2) is on average 50% of a homogeneous sample (N1). Fig. 5 shows the FESEM images of the two samples N1 and N2, after being placed in the charge and discharge cycles and completion of the work process. As can be seen in the figure, the N1 sample (sample with particle size less than 25 microns) has a more uniform appearance and morphology than the N2 sample. Heterogeneous distribution of particles will reduce battery life and cyclability. Even in practical conditions, after the electrode slurry made on the copper foil is coated, the coating obtained from the sample with particle size less than 25 microns is much softer and more uniform. In comparison, the sample with a particle size higher than 25 microns has a rough coating, which causes a potential difference, reducing the contact surface between the particles and the loss of the separator during the assembly process or the charge and discharge cycles.

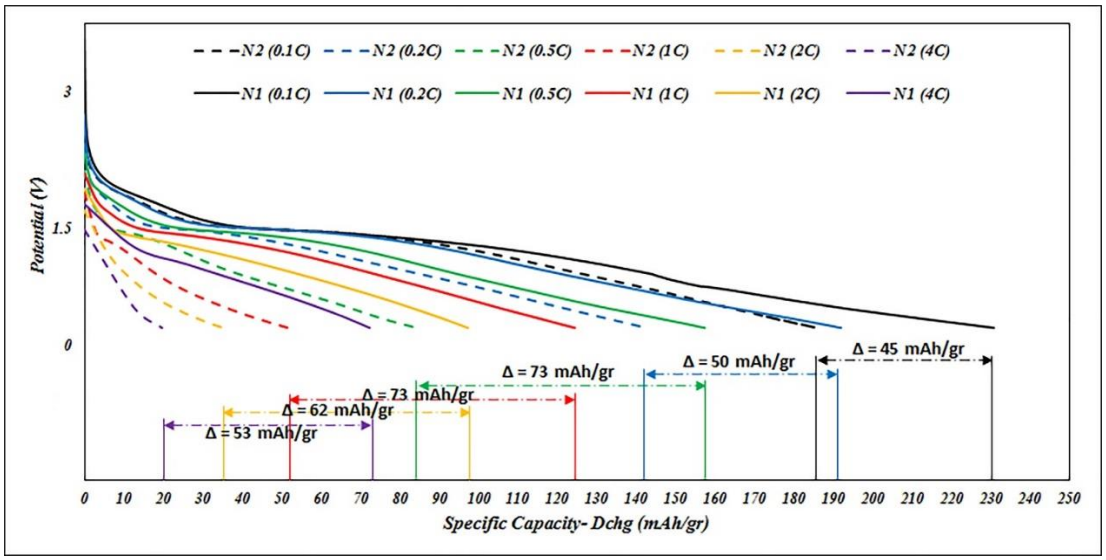

Fig. 4. Comparison of discharge diagrams of two samples N1 and N2.

Table 2. Electrochemical performance of the produced electrodes.

		No. of cycles per each crate						Capacity (mAh/g)					
Sample No.	Cycle No.	0.1C	0.2C	0.5C	1C	2C	4C	0.1C	0.2C	0.5C	1C	2C	4C
N1	179	4	8	23	48	48	48	231	192	157	124	97	72
N2	179	4	8	23	48	48	48	186	142	84	51	35	19

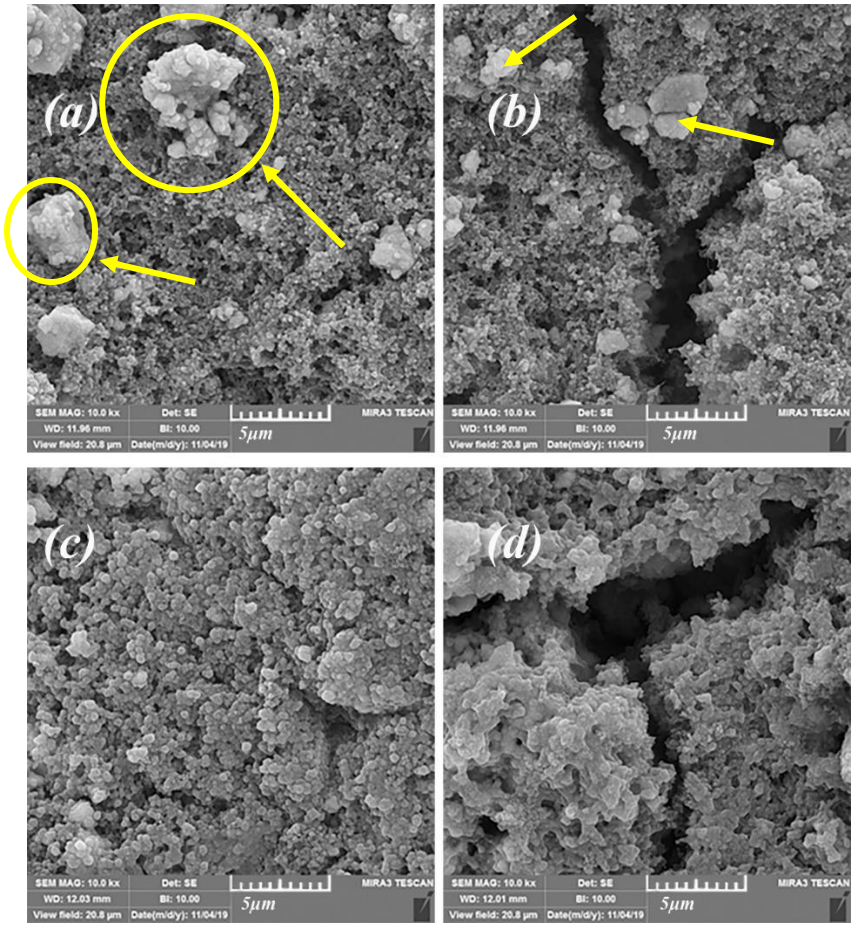

Fig. 5 (a, b) The morphological features of the N2, (c, d) The morphological features of the N1.

Figure 6 is a diagram of the cyclability of the two samples N1 and N2, which shows the difference in the capacity retention and cyclability of both samples and confirms the poor performance of sample N2.

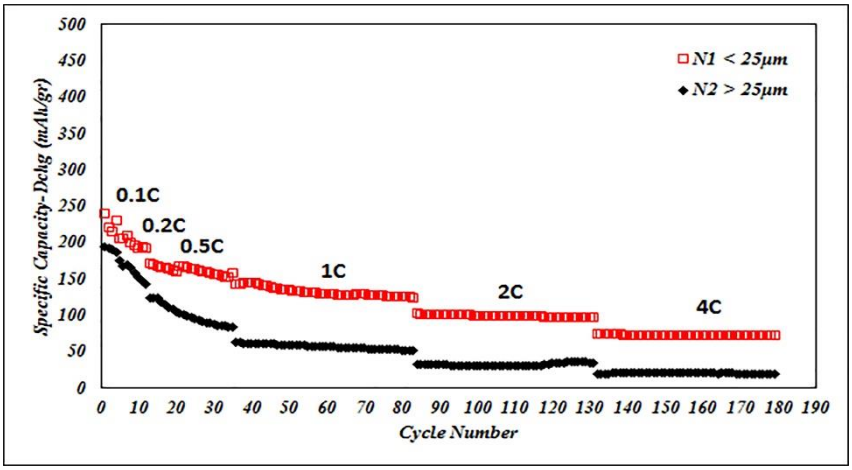

Fig. 6. Cyclic stability or cyclability of N1 and N2.

3.4. Electrochemical Properties

The electrochemical impedance (EIS) test is performed when the cell is totally discharged. Figure 7 shows the Nyquist diagrams of the sample with particle size less than 25 microns [13] and sample with a particle size of more than 25 microns (the corresponding curve is placed in the figure for performing the fitting process of lab data for the EIS test). An intercept is observed at high frequencies, followed by a semicircle in the medium frequency region and a straight line at a low frequency. Ohmic resistors (R_e) include electrolyte and electrode resistors seen as the intercept impedance in the Z' axis. The charging transfer resistors (R_{ct}), available between the anodic material and electrolyte, are in conformity with the diameter of the semicircle on the Z' axis. The tailbone or the straight line is connected with the emission of lithium ions in the electrode bulk, known as the Warburg diffusion (Z_w). Double layer strength and capacitive surface film are shown as the fixed phase element (CPE) [14,15].

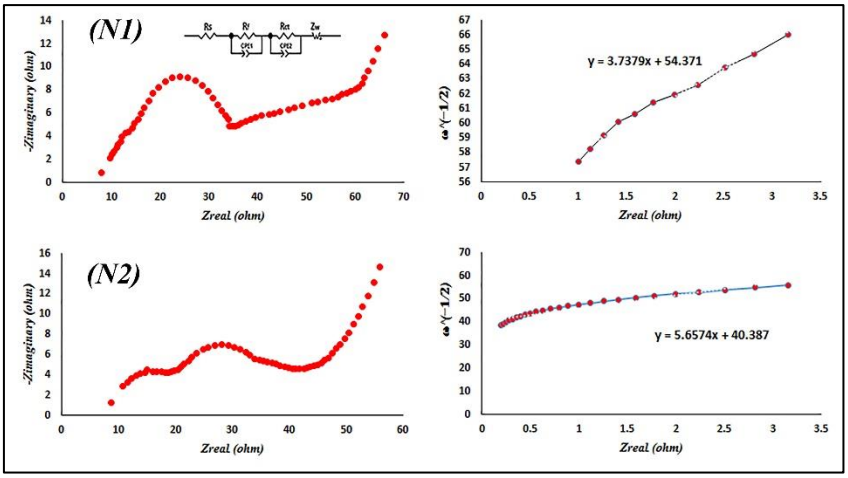

Fig. 7. EIS spectra of the sample with particle size less than 25 microns (N1) [13] and the sample with particle size more than 25 microns (N2)

Table 3 appears the fitting comes about of the impedance test of the tests. In this table, the Rct values of the sample with particle size less than 25 microns and the sample with particle size more than 25 microns are presented, which in N1 and N2 are equal to 29 and 51 $\Omega\ cm^2$, separately. Therefore, using Equation 2, the diffusion coefficient of lithium ions in each sample was calculated. According to the results, the emission rate of lithium-ion in the sample with particle size less than 25 microns is higher than the sample with a particle size of more than 25 microns, so that the diffusion coefficient in the N1 is equal to 1.24×10^{-11} cm^2/s, which is approximately 2.3 times the sample N2 with a diffusion coefficient of 5.42×10^{-12} cm^2/s.

Table 3. EIS parameters of the produced electrodes

Sample	R_e ($\Omega\ cm^2$)	R_{ct} ($\Omega\ cm^2$)	i_0 (mA cm^2)	σ_w ($\Omega\ cm^2\ s^{1/2}$)	D_c (cm^2/s)
N1	16.19	29	8.85×10^{-4}	3.74	1.24×10^{-11}
N2	8.76	51	5.03×10^{-4}	5.65	5.42×10^{-12}

4. Conclusion

In this study, we investigated the particle size distribution as an essential parameter in the performance of the $TiNb_2O_7$ anode. The presented results show the effect of shape and scale of particle size distribution on the performance of electrodes. In general, the smaller and more uniform the particle size distribution, the correlation and contact surface between the particles increase, and the faster displacement of lithium ions. Hence, the ability to maintain capacity at higher C rates will be better. Differences in particles size distributions resulted in variable discharge capacities so that the sample with a particle size of more than 25 microns showed a capacity of 19 mAh/g after 179 cycles, which had a lower capacity than their sample with particle size less than 25 microns. The final capacity of the sample with a particle size less than 25 microns is 72 mAh/g.

References

[1] Y. Liu, Y. Yang, "Recent progress of TiO_2-based anodes for Li ion batteries", Journal of Nanomaterials, vol. 2016, 2016, pp. 1-15.

[2] S. K. Balasingam, M. Kundu, B. Balakrishnan, H. Kim, A. M. Sevensson, K. Jayasayee, "Hematite microdisks as an alternative anode material for lithium-ion batteries", Materials Letters, vol. 247, 2019, pp. 163-166.

[3] S. Li, X. Cao, C. N. Schmidt, Q. Xu, E. Uchaker, Y. Pei, G. Cao, "$TiNb_2O_7$/graphene composites as high-rate anode materials for lithium/sodium ion batteries", Journal of Materials Chemistry A, vol. 4, 2016, pp. 4242-4251.
[4] X. Xia, Sh. Deng, Sh. Feng, J. Wu, J. Tu, "Hierarchical porous $Ti_2Nb_{10}O_{29}$ Nanospheres as superior anode materials for lithium-ion storage", Journal of Materials Chemistry A, vol. 5 2017, pp. 21134-21139.
[5] D. Pham-cong, J. Kim, V. T. Tran, S.J. Kim, S. Jeong, J. Choi, Ch. Cho, "Electrochemical behavior of interconnected $Ti_2Nb_{10}O_{29}$ nanoparticles for high-power Li-ion battery anodes", Electrochimica Acta, vol. 236, 2017, pp. 451-459.
[6] G. Zhu, Y. Wang, Y. Xia, "Ti-based compounds as anode materials for Li-ion batteries", Energy & Environmental Science, vol. 5, 2012, pp. 6652-6667.
[7] D. Aurbach, B. Markovsky, I. Weissman, E. Levi, Y. Ein-Eli, "On the correlation between surface chemistry and performance of graphite negative electrodes for Li ion batteries", Electrochimica Acta, vol. 45, 1999, pp. 67-86.
[8] B. Michalak, H. Sommer, D. Mannes, A. Kaestner, T. Brezesinski, J. Janek, "Gas Evolution in Operating Lithium-Ion Batteries Studied in Situ by Neutron Imaging", Scientific Reports, vol. 5, 2015, pp. 1-9.
[9] F. Rçder, S. Sonntag, D. Schrçder, U. Krewer, "Simulating the Impact of Particle Size Distribution on the Performance of Graphite Electrodes in Lithium-Ion Batteries", Energy Technology, vol. 4, 2016, pp. 1-11.
[10] Zh. Wu, W. Ren, L. Wen, L. Gao, J. Zhao, Z. Chen, G. Zhou, F. Li, H. Cheng, "Graphene Anchored with Co_3O_4 Nanoparticles as Anode of Lithium-Ion Batteries with Enhanced Reversible Capacity and Cyclic Performance", ACS Nano, vol. 4, 2010, pp. 3187-3194.
[11] G. T. Feya, Y. G. Chen, H. Kao, "Electrochemical properties of $LiFePO_4$ prepared via ball-milling", Journal of Power Sources, vol. 189, 2009, pp. 169-178.
[12] Th. Drezen, N. Kwon, P. Bowen, I. Teerlinck, M. Isono, I. Exnar, "Effect of particle size on $LiMnPO_4$ cathodes", Journal of Power Sources, vol. 189, 2009, pp. 169-178.
[13] T. Adhami, R. Ebrahimi-Kahrizsangi, H. R. Bakhsheshi-Rad, S. Majidi, M. Ghorbanzadeh, F. Berto, "Synthesis and electrochemical properties of $TiNb_2O_7$ and $Ti_2Nb_{10}O_{29}$ anodes under various annealing atmospheres", Metals, vol. 11, 2021, pp. 1-12.
[14] A. R. Madram, R. Daneshtalab, M. R. Sovizi, "Effect of Na^+ and K^+ co-doping on the structure and electrochemical behaviors of $LiFePO_4$/C cathode material for lithium-ion batteries", Royal Society of Chemistry, 2016, pp. 101477-101484.
[15] L. Buannic, J. Colin, Lise Daniel, S. Patoux, "Effect of syntheses and post synthetic treatments on mixed titanium niobium oxides for use as negative electrode in high power Li-ion batteries", Electrochemical Society, 2013.